Computer Methods and Programs in Biomedicine 153 (2018) 61–69

Contents lists available at ScienceDirect

Computer Methods and Programs in Biomedicine

journal homepage: www.elsevier.com/locate/cmpb

Recognition of pigment network pattern in dermoscopy images based on fuzzy classification of pixels

Jose Luis Garcia-Arroyo*, Begonya Garcia-Zapirain

Deustotech-LIFE Unit (eVIDA Research Group), University of Deusto Avda. Universidades, 24, 48007 Bilbao, Spain

ARTICLE INFO

Article history:
Received 28 June 2017
Revised 1 September 2017
Accepted 2 October 2017

Keywords:
Pattern recognition
Image processing
Machine learning
Fuzzy classification
Alpha-cuts
Reticular pattern
Dermoscopic structure

ABSTRACT

Background and Objective: One of the most relevant dermoscopic patterns is the pigment network. An innovative method of pattern recognition is presented for its detection in dermoscopy images.
Methods: It consists of two steps. In the first one, by means of a supervised machine learning process and after performing the extraction of different colour and texture features, a fuzzy classification of pixels into the three categories present in the pattern's definition ("net", "hole" and "other") is carried out. This enables the three corresponding fuzzy sets to be created and, as a result, the three probability images that map them out are generated. In the second step, the pigment network pattern is characterised from a parameterisation process –derived from the system specification– and the subsequent extraction of different features calculated from the combinations of image masks extracted from the probability images, corresponding to the alpha-cuts obtained from the fuzzy sets.
Results: The method was tested on a database of 875 images –by far the largest used in the state of the art to detect pigment network– extracted from a public Atlas of Dermoscopy, obtaining AUC results of 0.912 and 88%% accuracy, with 90.71%% sensitivity and 83.44%% specificity.
Conclusion: The main contribution of this method is the very design of the algorithm, highly innovative, which could also be used to deal with other pattern recognition problems of a similar nature. Other contributions are: 1. The good performance in discriminating between the pattern and the disturbing artefacts –which means that no prior preprocessing is required in this method– and between the pattern and other dermoscopic patterns; 2. It puts forward a new methodological approach for work of this kind, introducing the system specification as a required step prior to algorithm design and development, being this specification the basis for a required parameterisation –in the form of configurable parameters (with their value ranges) and set threshold values– of the algorithm and the subsequent conducting of the experiments.

1. Introduction

Dermoscopy is a widely-used technique in the early detection of melanoma. It enables the in-depth visualisation of structures, forms and colours that are not accessible through simple visual inspection, and also allows reproducibility in the diagnosis and the use of digital image processing techniques [1]. The most relevant indicators are dermoscopic patterns or structures [1], whereby a Computer Aided Diagnosis (CAD) system should deal with their recognition [2–4]. It is a complex issue as, on the one hand, from the point of view of image processing, it is a difficult problem to deal with and, on the other, its objectivation is difficult since, on many occasions, assessment by human experts is rather subjective [5]. Nonetheless, given its importance, some good methods have already been developed for many of the patterns [6–9].

One of the most relevant dermoscopic patterns is the pigment network [1], also known as the reticular pattern, whose presence is an indicator of the existence of melanin deep inside the layers of the skin. It is an important criterion for the purpose of discerning whether a lesion is melanocytic or not and an important indicator in the diagnosis of melanoma [1]. The name derives from the form of this structure, which resembles a net, darker in colour than the "holes" it forms, corresponding to the lesion's background [1]. There are two types of pigment network: typical (relatively uniform, regularly meshed, homogeneous in colour and usually thinning out at the periphery [10]) and atypical (non-uniform, with

* Corresponding author.
E-mail addresses: jlgarcia@deusto.es (J.L. Garcia-Arroyo), mbgarciazapi@deusto.es (B. Garcia-Zapirain).

https://doi.org/10.1016/j.cmpb.2017.10.005

darker and/or broadened lines and "holes" that are heterogeneous in diameter and shape, these being the lines are often hyperpigmented and may end abruptly at the periphery [10]), the latter often being an indicator of malignancy [1]. Examples of pigment network can be seen in Figs. 3, 4, 7 and 8.

Recognition of pigment network pattern is a complex issue. On the one hand, what sometimes occurs is that there is little contrast between the network and the background. On the other, errors are common insofar as the pigment network may be confused with other dermoscopic structures such as globules or streaks, or with artefacts such as hair, ruler markings or even bubbles. Thus, and although several good methods have been described in recent years, this remains a challenging problem.

This work presents an innovative method for recognition of pigment network pattern in dermoscopy images. This method can also be used to help deal with other problems involving pattern recognition of a similar nature.

1.1. State of the art

A thorough revision of the state of the art has been conducted by the authors, which is shown in detail in [11], to which 3 recent works are added here. Numerous are the imaging techniques that have been used, as will be seen. After analyzing the most relevant works of reticular pattern recognition we can consider that the algorithms consist, roughly, of two steps.

Firstly, a mask candidate to be the reticular structure is obtained. For this, usually a transformation of the image is made to the grayscale followed by different techniques: line detection [12–16], thresholding [12,17–19], spectral features –mostly high-pass filters– [15,18–25], gray level co-occurence matrix (GLCM) [21,24,26,27], local binary pattern (LBP) [16,28], snakes [13], Laws' energy masks [27,29], neighborhood gray level dependence matrix (NGLDM) [29], Markov random fields (MRF) [7,30], discrete wavelet frame(DWF) [28], steerable pyramids transformation (SPT) [8] and curvelet transformation [31]. Sometimes combined with color features [8,16,19,20,22,24,28]. In most of works, from the generated mask a post-processing process is performed using morphological techniques.

Secondly, as the main objective of most of the studies is also determining whether or not it has a reticular pattern, then most of them include morphological/structural/geometric characterisations of the pigment network [14,15,17,19–27,29,31] and, in some cases, mapping of the network structure to a graph-based estructure [20,21,25]. Sometimes chromatic features are used [8,16,19,20,22,24,28,30]. Finally, this is fed into a supervised machine learning process by performing either an empirical selection of threshold values or using a statistical function or a classifier.

Below are described the studies deemed most relevant by the authors in pigment network recognition, with a high number of images available for testing and the highest rates of reliability: 1. Sadeghi et al. [20], in which, following use of the Laplacian of Gaussian (LoG) filter and a subsequent processing, a graph structure is obtained from which a feature known as "density ratio" is calculated, which indicates the presence/absence of the pattern; 2. Barata et al. [23], in which, following use of a bank of directional filters and subsequent processing, five different morphological features are calculated, characterising the pigment network for its recognition; 3. Garcia-Arroyo et al. [24], in which a supervised machine learning process on a pixel level is carried out in order to obtain a mask with the candidate pixels to be part of the pigment network, which is subsequently processed using structural analysis, and finally making the pigment network recognition. In 4 are shown the results obtained in each of these three works and are also compared to the proposed method.

1.1.1. Contribution

Despite the importance of previous works, pigment network recognition remains a challenging problem and the proposed work attempts to address some of the shortcomings identified by the authors in the state of the art. The main contribution made by our work is the innovative design of the pattern recognition method, based on fuzzy classification of image pixels, which could also be used to deal with other pattern recognition problems of a similar nature. Moreover, it provides other improvements over other previous works, as will be commented in Section 4.1.

2. Materials and methods

2.1. Image database

The image database contains 875 images randomly extracted from the Interactive Atlas of Dermoscopy [32], used in the vast majority of important studies on dermoscopic pattern recognition. The image size is 768×512 pixels, with 10x increase and 72 ppi resolution, and is high-quality compressed in JPG format. All the images are labelled in relation to the pigment network pattern as belonging to "absent" or "present" categories, taken according to the diagnosis presented in the Atlas, carried out by expert dermatologists.

2.2. Specification of the system

In most works relating to pattern recognition from dermoscopy images, the description in medical language is provided as a specification of the system, and this is written in a language that is not deemed to be too formal. Hence, it is quite common in establishing what the method actually attempts to do to analyse the System Design section and, on many occasions, even the Results section too. To improve on this, the proposed work puts forward a new methodological approach for methods of this kind, introducing the system specification as a required step prior to algorithm design and development, being this specification the basis for a required parameterisation process which supports the design and development of the algorithm and the realisation of the experiments. This specification is carried out using the pattern' s definition itself, the exhaustive study of the dermoscopy images obtained from the database, the information provided by expert dermatologists and the labelling carried out by the latter. This new approach constitutes an attempt to formalise the design of dermoscopic pattern recognition methods in a more optimal way.

This specification can be carried out in different ways. In this work was made in the form of a set of requirements in structured natural language: 1. For an image to have a pigment network pattern, it must contain a structure of this type in some part of the lesion. This structure is a net shape, which is light brown, dark brown, grey or black in colour, the "holes" being a lighter colour than the "net". In some cases, there may be little contrast or the net is faint; 2. The texture is highly characteristic, both in "net" and "hole" type pixels; 3. This net shape comprises one or more structures in the shape of a net (subnets), with one or more cells together in each one, making a total of cells greater or equal than two; 4. Even though the mesh width of the net differs within the same lesion (particularly in atypical cases), the width is normally similar on a local scale. Likewise, even though the cells may be different sizes within the same lesion (particularly in atypical cases), they are normally consistent in size with others on a local scale; 5. On a global level for the set of images used, there is a range for such sizes corresponding to the characteristics of the images being studied (in the event of these changing, the ranges would also change); 6. There are some images in which it is very difficult to discern the pattern, even for a human expert. In addition, due to

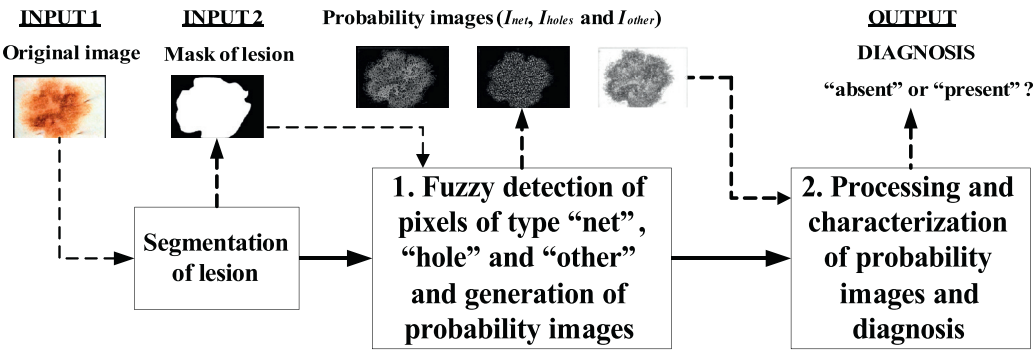

Fig. 1. High level view of the System Design.

the subjectivity of assessment by experts, there are some "borderline images" where, despite the system operating properly, there may be an incorrect diagnosis in relation to prior labelling.

These requirements, as well as making up the system specification, also form the basis for conducting the parameterisation process –in the form of configurable parameters (with their value ranges) and set threshold values–, which will be explained in Sections 2.6.1 and 2.6.2.

2.3. Motivation behind the fuzzy classification of pixels

The algorithm is designed from the specification, and this design, broadly speaking, consists of a pixel classification in the three categories present in the pattern's definition ("net", "hole" and "other"), followed by processing of the regions corresponding to the aforementioned categories based on the pattern' s description, in order to perform its recognition.

If the different cases of images are examined (e.g. in Figs. 3, 4, 7 and 8), it can be ascertained that the pixel features of colour and texture vary hugely in the different images and in the different pigment network structures, meaning that a pixel with certain features corresponds to a category in one place and that another pixel with the same features corresponds to another category in another place. Thus, a hard classification of pixels does not adapt well to the problem, so the most suitable approach is to carry out a soft or fuzzy classification, undertaken here. Consequently, the three regions obtained will be of fuzzy type, and this is implemented here generating three probability images that will later be processed.

2.4. High level view of the system design

Here is shown the High level view of the system design, a detailed explanation of which is provided in Sections 2.5 and 2.6. As shown in Fig. 1, firstly, **Segmentation of lesion** is performed, with the original and segmented images therefore being the system' s inputs, comprising two modules: **1. Fuzzy detection of pixels of type "net", "hole" and "other" and generating probability images**, where three probability images I_{net}, I_{holes} and I_{other} are generated from the original image I, corresponding the value of every pixel (x, y) in each image to the probability of its belonging to "net", "hole" and "other" respectively in I. **2. Processing and characterisation of probability images and diagnosis**, where following processing of the probability images and their subsequent characterisation the diagnosis is conducted, differentiating between "absent" and "present", which is the system output.

2.4.1. Image preprocessing not performed

Prior preprocessing of the image in most dermoscopic pattern recognition methods is carried out in order to detect and eliminate any disturbing artefacts, such as hair, flashes, ruler markings or air bubbles. This is on occasions a source of errors as groups of pixels that form part of the pattern may be incorrectly recognised as part of the artefacts. To avoid this, no prior preprocessing is undertaken in this method and, therefore, the possible presence of disturbing artefacts is taken into account in the pattern recognition algorithm itself.

2.4.2. Segmentation of lesion

As can be seen in Fig. 1, the image is initially segmented. The authors of this work have developed a segmentation algorithm that provides very good results [33]. Nonetheless, the lesions were manually segmented –by the first author with the guidelines and validation of the collaborating dermatologists– in order to isolate development and testing of the proposed pattern recognition method with regard to how this algorithm works –and also taking into account that this algorithm has been created in order to be integrated into a CAD for the automated detection of melanoma that includes the task of segmentation–. In any event, it should be pointed out that the pattern recognition method itself may obtain the structure detected without the need for such prior knowledge, which is only deemed necessary to prevent the effect that may give rise to the possible presence, normally very fine and faint, of pigmented net structures on the skin outside the lesion –which will only give problems to the recognition method in very rare cases, in lesions that are also labeled as "absent"–.

2.5. Module 1: fuzzy detection of pixels of type "net", "hole" and "other" and generating probability images

2.5.1. Outline of Module 1

In this module, the dermoscopy image pixels are fuzzy classified into "net", "hole" and "other" categories by means of a supervised machine learning process, which enables the corresponding three probability images to be generated. As can be seen in Fig. 2, this module comprises 4 phases. Firstly, pixel samples are taken and labelled into the three different categories. Secondly, a set of features that are suitable for discrimination is extracted. Thirdly, this enables a fuzzy classifier to be used in order to generate a fuzzy classification model, assigning to every pixel (x, y) a probability value belonging to each category. This in turn enables three fuzzy sets μ_{net}, μ_{holes} and μ_{other} to be created on the set of pixels. Lastly, the three probability images I_{net}, I_{holes} and I_{other} are constructed from these fuzzy sets.

2.5.2. Setting the training data (Module 1.1)

Samples of pixels from 50 images of different types ("absent" and "present") were selected, which were labelled in "net", "'hole" and "other" categories corresponding to the pixels that are in the net, those in the holes and others. Attempts were made to ensure

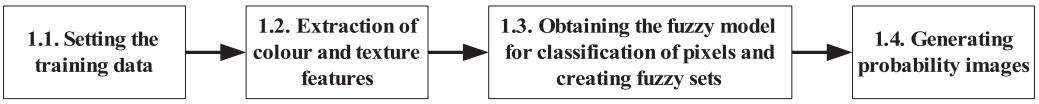

Fig. 2. Phases of the fuzzy detection of "net", "hole" and "other" pixel types and generating probability images module.

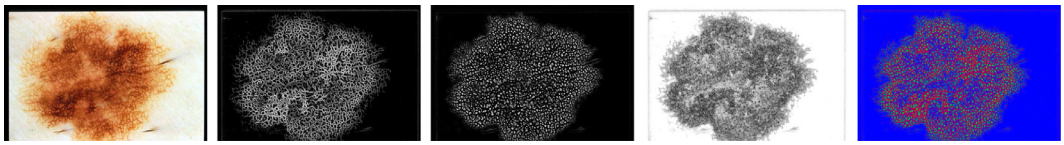

Fig. 3. Example of processing in the fuzzy detection of pixels of type "net", "hole" and "other" and generating probability images. The first image is the original I. The following three are the grey probability images I_{net}, I_{holes} and I_{other}. The fifth is the colour image $I_{net\_holes\_other}$.

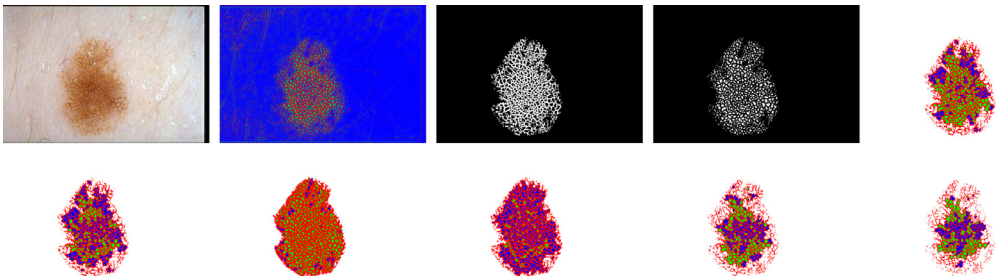

Fig. 4. Example of the motivation behind the combinations of image masks obtained from probability images corresponding to the $\alpha - cuts$ obtained from the fuzzy sets in an image with pigment network: 1: Original image; 2: $I_{net\_holes\_other}$; 3: $BW^{0.3}_{net}$; 4: $BW^{0.3}_{holes}$; The others are images of pigment network detection, corresponding to different values of (α_{net}, α_{holes}, $prop$). 5 and 6: $I^{(0.3,0.3)}_{PN}[0.7]$ and $I^{(0.3,0.3)}_{PN}[0.8]$ respectively, note that $prop = 0.7$ in the first and $prop = 0.8$ in the second; 7, 8, 9 and 10: $I^{(0.1,0.1)}_{PN}[0.9]$, $I^{(0.2,0.5)}_{PN}[0.8]$, $I^{(0.4,0.3)}_{PN}[0.7]$ and $I^{(0.5,0.3)}_{PN}[0.6]$.

that the number of sampled pixels was reasonably balanced in relation to sample size in the three categories and also, as far as possible, in relation to the different case studies existing in each category, with regard to the types and sizes of nets and holes in the case of "net" and "hole", and by selecting examples of pixels belonging to the skin, other dermoscopic structures and artefacts (noise) such as hair, rulers, flashes and air bubbles in the case of "other". In any event, as shall be seen, the method has a self-correcting mechanism in its actual design in order to address different ways of carrying out this sampling process.

2.5.3. Extraction of colour and texture features (Module 1.2)

A set of color and texture features is extracted in order to characterize the pixels, with a view to discriminating between categories as far as possible [34,35]. 159 features are extracted in total, of the following two types:

Colour features. 16 color features are extracted corresponding to the gray value and to the values of the different channels RGB, rgb (normalized RGB), HSV, CIEXYZ, CIELab and CIELuv color spaces [34].

Texture features. 143 texture features are extracted from the image converted to gray using the formula $I_G(x,y) = \frac{1}{3}I_{red}(x,y) + \frac{1}{3}I_{green}(x,y) + \frac{1}{3}I_{blue}(x,y)$. Values are extracted both from the gray image and from the blurred images resulting from application of a Gaussian filter bank, using the formula [34]: $G_\sigma(x,y) = \frac{1}{2\pi\sigma^2}e^{-\frac{x^2+y^2}{2\sigma^2}}$, with σ values of the form $\sigma = 2^m$, with $m = 0, 1, 2, \ldots, m_{max}$ and $m_{max} = 4$.

- *Pixel values:* 5 features are extracted corresponding to the value of each pixel: 1 for each σ (the one corresponding to the gray image is considered to be a color feature).
- *Sobel filter:* 6 features are extracted, corresponding to the gradient at each pixel [34]: 1 ++ 1 for each σ.
- *Difference of Gaussian ("DoG"):* 10 features are extracted for the different pairs of values (σ_i, σ_j), such as $i > j$ and $\sigma_m = 2^m$, with $m = 0, 1, \ldots, m_{max}$, and the different [35] $DoG_{\sigma_i\sigma_j}(x,y) = G_{\sigma_i}(x,y) - G_{\sigma_j}(x,y)$ are applied: corresponding to the different combinations of (σ_i, σ_j).
- *Laplacian filter:* 5 features are extracted, calculating the Laplacian [35] at each pixel: 1 for each σ.
- *Hessian matrix:* 48 features are extracted, firstly obtaining the Hessian matrix at each pixel and then calculating 8 different features from it [35]: 8 ++ 8 for each σ.
- *Texture statistics:* 25 features are extracted, with different statistics within a radius of σ from each pixel (mean, variance, median, minimum and maximum) being calculated [35]: 5 for each σ.
- *Gabor filters:* 44 features are extracted, with different Gabor filters [35] being calculated at each pixel in the gray image corresponding to different values of the parameters λ, θ, ψ, σ and γ.

2.5.4. Obtaining the fuzzy model for classification of pixels and creating fuzzy sets (Module 1.3)

A fuzzy classifier is used to generate a fuzzy classification model from the values of labelled pixels in the different categories obtained from the extraction of colour and texture features. This model enables the probabilities of belonging to the "net", "hole" and "other" categories to be ascertained for each pixel of the image I. The classifier used and the results obtained are explained in Section 3.1.

If we consider the image I to be of $w \times h$ in size and we define the set of pixels $X = [0, w-1] \times [0, h-1]$, we can then define three fuzzy sets of X as follows. $\mu_{net} : X \to [0,1]$, $\mu_{holes} : X \to [0,1]$ and $\mu_{other} : X \to [0,1]$, such that for each pixel $(x, y) \in X$ the values $\mu_{net}(x, y)$, $\mu_{holes}(x, y)$ and $\mu_{other}(x, y)$ are the probabilities given by the fuzzy classification. These fuzzy sets meet two criteria: firstly, they are not null, i.e. that $\Sigma_{(x,y)\in X}\mu_{net}(x, y) > 0$, $\Sigma_{(x,y)\in X}\mu_{holes}(x,$

$y) > 0$ and $\Sigma_{(x,\,y)\in X}\mu_{other}(x,\,y) > 0$ are met and, secondly, that $\forall(x,\,y)\in X,\ \mu_{net}(x,y)+\mu_{holes}(x,y)+\mu_{other}(x,y)=1$ is met. Thus, we can consider the family of fuzzy sets $\{\mu_{net},\ \mu_{holes},\ \mu_{other}\}$ to be a fuzzy partition of X.

2.5.5. Generating probability images (Module 1.4)

From the fuzzy sets μ_{net}, μ_{holes} and μ_{other} three grey probability images are generated I_{net}, I_{holes} and I_{other} of $w\times h$ in size and a greyscale in [0, 255]. These are defined as follows: $\forall(x,\,y)\in X,\quad I_{net}(x,y)=255.\mu_{net}(x,y),\quad I_{holes}(x,y)=255.\mu_{holes}(x,y)$ and $I_{other}(x,y)=255.\mu_{other}(x,y)$. Evidently, $\forall(x,\ y)\in X$, $I_{net}(x,y)+I_{holes}(x,y)+I_{other}(x,y)=255$.

These probability images show the pixel probabilities in graphic form. Moreover, taking advantage of the fact that there are three images, a colour image $I_{net\_holes\_other}$ can be built by assigning the I_{net} to the red channel, I_{holes} to the green channel and I_{other} to the blue channel. This new image is equivalent to the three probability images and enables the result of the fuzzy classification of pixels to be seen much more clearly in graphic form, all of which is shown in Fig. 3.

2.6. Module 2: processing and characterisation of probability images and diagnosis

2.6.1. Motivation behind the combinations of image masks obtained from probability images corresponding to the $\alpha-cuts$ obtained from the fuzzy sets. Parameters α_{net}, α_{holes} and prop

The initial idea of the algorithm was, broadly speaking, to obtain the masks BW_{net}, BW_{holes} and BW_{other} corresponding to the pixels which are hard-classified into the "net", "hole" and "other" categories and then look for the pigment network holes in the holes of BW_{net} that coincide "approximately" with their intersection with BW_{holes}. This meant that, firstly, the mask $BW_{holesofnet}$ is obtained from BW_{net}, corresponding to the union of the holes of BW_{net} (i.e. the union of the 8-connected components $C_{holesofnet}\subset\complement(BW_{net})$ that do not touch the edge of the image) and, secondly, the "approximately" corresponds to a threshold value of proportion thr_prop set beforehand, which determines that those $C_{holesofnet}$ such as $\frac{|C_{holesofnet}\cap BW_{holes}|}{|C_{holesofnet}|} > thr\_prop$ are selected as holes corresponding to the pigment network. It is an innovative idea, but with the problem that, as has been explained in Section 2.3, the hard classification does not adapt well to recognition of this pattern, which is fuzzy in nature, the same as setting a single value thr_prop for the hole selection.

Therefore, a variation on the initial idea was made using a fuzzy approach. On the one hand, thr_prop can be parameterised so as to take different values $prop$. On the other, from the probability images I_{net} and I_{holes} corresponding to the fuzzy sets μ_{net} and μ_{holes}, obtained in module 1, image masks can be extracted, corresponding to $\alpha-cuts$ obtained from the fuzzy sets for different probability values α_{net} and α_{holes}, and subsequently combined, as follows.

Defining a $\alpha-cut\ [\mu]_\alpha\subset X$, given a fuzzy set μ of a set X and a value $0\le\alpha\le1$, as $[\mu]_\alpha=\{(x,y)\in X:\mu(x,y)\le\alpha\}$, we have the masks: $BW_{net}^{\alpha_{net}}=\{(x,y)\in X: I_{net}(x,y)\le 255.\alpha_{net}\}$, extracted from I_{net} and corresponding to $[\mu_{net}]_{\alpha_{net}}$, and $BW_{holes}^{\alpha_{holes}}=\{(x,y)\in X: I_{holes}(x,\,y)\le 255.\alpha_{holes}\}$, extracted from I_{holes} and corresponding to $[\mu_{holes}]_{\alpha_{holes}}$. These masks can be combined in such a way that the initial idea can be applied for each combination of (α_{net}, α_{holes}, $prop$), obtaining a set of selected holes as a result. The result of each combination can be seen graphically by building a colour image of pigment network detection $I_{PN}^{(\alpha_{net},\alpha_{holes})}[prop]$ with $BW_{net}^{\alpha_{net}}$ in red and the 8-connected components $C_{holesofnet}^{\alpha_{net}}\subset BW_{holesofnet}^{\alpha_{net}}$ (holes of $BW_{net}^{\alpha_{net}}$) in blue or green, according to whether $\frac{|C_{holesofnet}^{\alpha_{net}}\cap BW_{holes}^{\alpha_{holes}}|}{|C_{holesofnet}^{\alpha_{net}}|}$ is $\le prop$ (unselected holes) or $> prop$ (selected). Fig. 4 shows a graphic example of this.

In order to include the relevant case studies of the parameters α_{net}, α_{holes} and $prop$ (renamed here as α_{net}^{i}, α_{holes}^{j} and $prop^{k}$ respectively), the following possible values are chosen: 1. $(0.1\le\alpha_{net}^{i}\le0.9)$ with $i=0,1,\ldots,8$ and satisfying $\alpha_{net}^{i+1}-\alpha_{net}^{i}=0.1\ \ \forall i$; 2. $(0.1\le\alpha_{holes}^{j}\le0.9)$ with $j=0,1,\ldots,8$ and satisfying $\alpha_{holes}^{j+1}-\alpha_{holes}^{j}=0.1\ \ \forall j$; 3. $(0.5\le prop^{k}\le0.9)$ with $k=0,1,\ldots,4$ and satisfying $prop^{k+1}-prop^{k}=0.1\ \forall k$.

It can be observed intuitively that for each part of a pigment network (net and holes) of an image, there are different values of (α_{net}, α_{holes}, $prop$) such that this part may be detected, in the sense that there are selected holes –the holes in green present in $I_{PN}^{(\alpha_{net},\alpha_{holes})}[prop]$, as shown in Fig. 4 (5–10)– connected to a selected net mesh. It can also be seen that in the images that have no pigment network, selected holes tend not to be obtained as soon as the values of probability rise slightly. It is important to point out that this algorithm entails a self-correcting effect against the result of the supervised machine learning process performed in the first module since, even though the pixel probability distribution of being in the net, holes or other varies, the method continues to work properly, which makes this method very robust in terms of the pixel sampling process.

As shall be seen, discrimination between "absent" and "present" made in the module 2 is based on the basic idea for the detection of pigment network presented here, adding the parameterisation obtained from the system specification, shown in Section 2.6.2.

2.6.2. Motivation behind parameterisation obtained from the system specification. Parameters numMinHoles, distMaxHoles and rangMaxSizeHole. Threshold values thr_minHoleSize, thr_maxHoleSize and thr_numMinTotalHoles

The parameterisation process is carried out based on the system specification shown in Section 2.2. The parameters α_{net}, α_{holes} and $prop$, described in Section 2.6.1 arise from requirements 1 and 2 regarding the definition and characterisation of net and holes. The threshold value $thr\_numMinTotalHoles=2$ is set from requirement 3. The subnet concept arises from requirement 3 and the characterisation of a subnet from three parameters is obtained from requirements 3 and 4: $numMinHoles$ corresponding to the minimum number of holes that each subnet must have, $distMaxHoles$ corresponding to the maximum distance there must be between the subnet hole centroids and $rangMaxSizeHole$ corresponding to the uniformity of subnet hole sizes. This is understood as meaning that if $meanSizeHoles$ is the mean subnet hole size, then the sizes of all the holes must be between $(1-rangMaxSizeHole).meanSizeHoles$ and $(1+rangMaxSizeHole).meanSizeHoles$, which in turn means that the ratio of sizes $size1$ and $size2$ between any two subnet holes must satisfy $\frac{size1}{size2}\le\frac{(1+rangMaxSizeHole)}{(1-rangMaxSizeHole)}$. The following values are considered for these parameters in this work: for $numMinHoles$: 1, 2 and 3, for $distMaxHoles$: 10, 15, 20 and 25 and for $rangMaxSizeHole$: 0.5, 0.65 and 0.8. The threshold values $thr\_minHoleSize=10$ and $thr\_maxHoleSize=200$ are experimentally set from requirement 5 in order to establish a wide range, meaning only the holes whose size is within this range are taken into consideration. Requirement 6 is taken into account in the design of the whole system.

2.6.3. Outline of Module 2

In this module, a supervised machine learning process is performed in order to carry out the diagnosis using the labelling from the database conducted by experts in relation to the pigment network pattern between "absent" and "present", described in Section 2.1. As can be seen in Fig. 5, this module comprises 3 phases. Firstly, different hard classification models corresponding

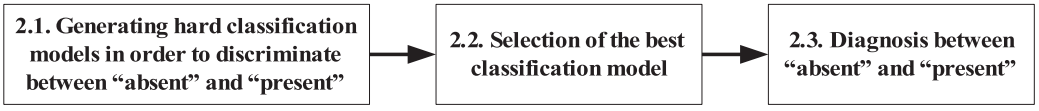

Fig. 5. Phases of processing and characterisation of probability images and diagnosis.

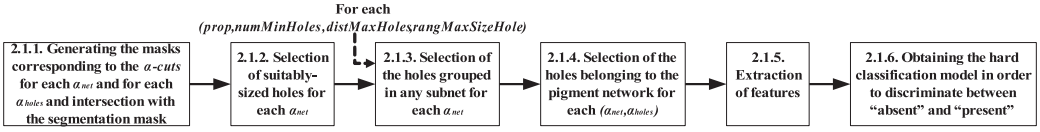

Fig. 6. Tasks performed in order to generate each classification model in the phase of generating hard classification models.

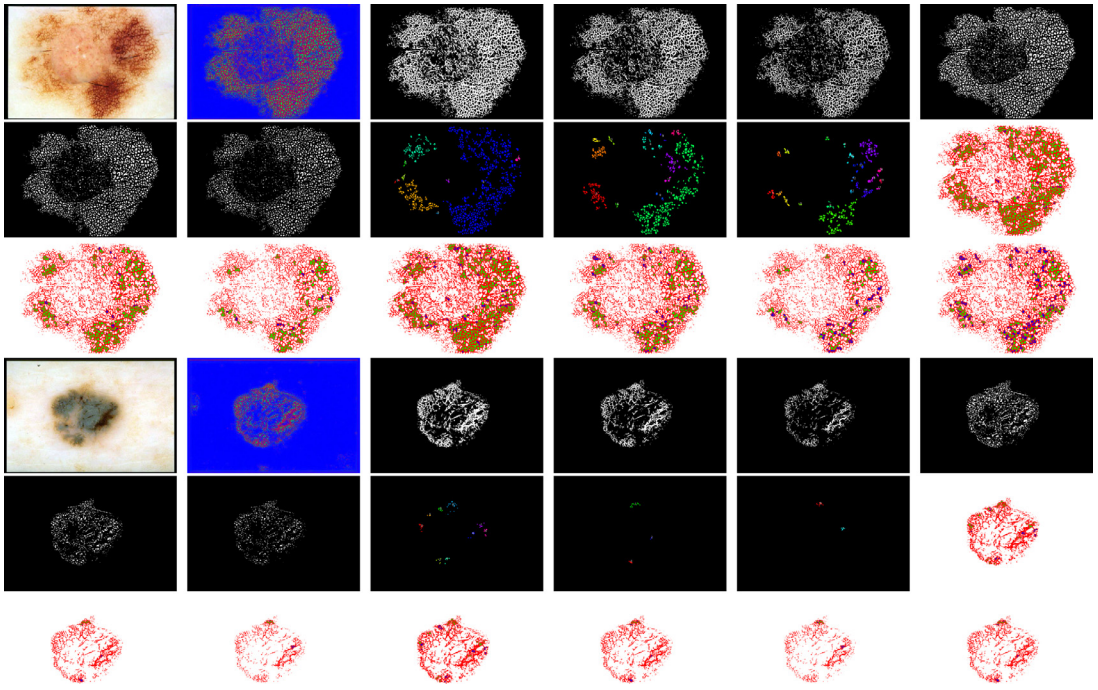

Fig. 7. Several examples of processing on two images in tasks 1–4. First image: an image with pigment network: 1: Original image; 2: $I_{net\_holes\_other}$ after module 1; 3, 4, 5, 6, 7 and 8: $BW_{net}^{0.3}$, $BW_{net}^{0.4}$, $BW_{net}^{0.5}$, $BW_{holes}^{0.3}$, $BW_{holes}^{0.4}$ and $BW_{holes}^{0.5}$ obtained in task 1 of phase 1; Before starting the task 3 is set: $(prop, numMinHoles, distMaxHoles, rangMaxSizeHole) = (0.5, 2, 20, 0.8)$. 9, 10 and 11: modification of the $BW_{holesofnet}^{\alpha_{net}}$ corresponding to the previous $BW_{net}^{\alpha_{net}}$, for parameters $(numMinHoles, distMaxHoles, rangMaxSizeHole) = (2, 20, 0.8)$, after task 3, showing the results in the images of sets of subnets: $I_{setofsubnets}^{0.3}$, $I_{setofsubnets}^{0.4}$ and $I_{setofsubnets}^{0.5}$; 12, 13, 14, 15, 16, 17 and 18: images of pigment network detection generated in the task 4, corresponding to the previous $BW_{holesofnet}^{\alpha_{net}}$ and $BW_{holes}^{\alpha_{holes}}$ and to $prop = 0.5$, i.e. $(prop, numMinHoles, distMaxHoles, rangMaxSizeHole) = (0.5, 2, 20, 0.8)$ set before starting the task 3, as commented: $I_{PN}^{(0.3.0.3)}$, $I_{PN}^{(0.4.0.3)}$, $I_{PN}^{(0.5.0.3)}$, $I_{PN}^{(0.3.0.4)}$, $I_{PN}^{(0.4.0.4)}$, $I_{PN}^{(0.5.0.4)}$ and $I_{PN}^{(0.4.0.5)}$. Second image: an image with faint pigment network: 19–36: The same values as for the above.

to different combinations of values of (*prop, numMinHoles, distMaxHoles, rangMaxSizeHole*) are generated, as will be shown. Secondly, the best classification model is then selected. Thirdly, this enables the diagnosis to be made, so that the images may be discriminated between "absent" and "present".

2.6.4. Generating hard classification models in order to discriminate between "absent" and "present" (Module 2.1)

In this phase, different hard classification models to discriminate between "absent" and "present" corresponding to different combinations of values of (*prop, numMinHoles, distMaxHoles, rangMaxSizeHole*) are generated from the set of images. According to the possible numerical values set for the parameters, the number of classification models generated is: $180 = 5 * 3 * 4 * 3$. As shown in Fig. 6, 6 tasks are involved in generating each one, which will be explained below. The first 2 tasks only need to be done 1 time, whereas the 4 following tasks are done 180 times, once for each combination of parameters.

Generating the masks corresponding to the $\alpha - cuts$ for each α_{net} and for each α_{holes} and intersection with the segmentation mask (Module 2.1.1). The different $BW_{net}^{\alpha_{net}}$ and $BW_{holesofnet}^{\alpha_{net}}$ corresponding to the $\alpha - cuts$ for each value α_{net} are generated from the image I_{net}, as described in Section 2.6.1. Similarly, from I_{holes}, the different $BW_{holes}^{\alpha_{holes}}$ corresponding to the $\alpha - cuts$ for each value α_{holes} are generated. Finally, all the generated masks are intersected with the segmentation mask. As a result of this task, and given the possible numerical values established, 9 masks of each type are created.

Selection of suitably-sized holes for each α_{net} (Module 2.1.2). Performed for each of the masks $BW_{holesofnet}^{\alpha_{net}}$. Suitably-sized holes $C_{holesofnet}^{\alpha_{net}}$ are selected, i.e. those meeting the condition $thr\_minHoleSize \leq |C_{holesofnet}^{\alpha_{net}}| \; thr\_maxHoleSize$, as commented in Section 2.6.2. As a result of this task, there is a modification of the $BW_{holesofnet}^{\alpha_{net}}$.

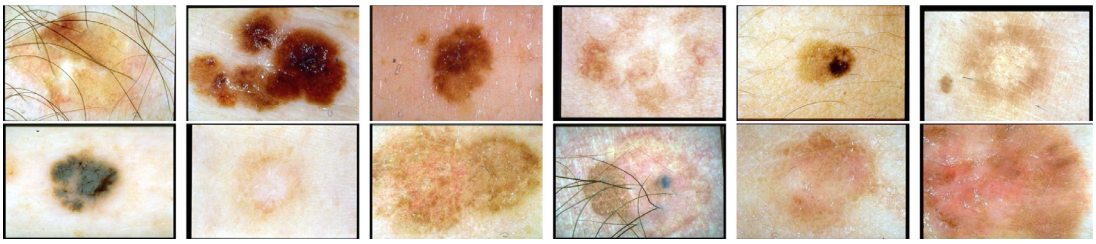

Fig. 8. Some examples of the diagnosis made by the proposed system, with difficult images. 1–7 are TP (True Positive): 1: hairy image; 2 and 3: oily images; 4, 5, 6 and 7: low contrast and the net is very faint, and in addition in 7 there are few holes (this image is also commented on in Fig. 7). 8 is FN (False Negative): contrast too low, the pattern is barely discernible, example of "borderline image". 9 is FP (False Positive): it has also a barely discernible pigment network, although in this case it has been labelled as "absent" by experts, another example of "borderline image". 10–12 are TN (True Negative): all the three images have similar textures to pigment network, 10 is a hairy image, 11 and 12 are oily images.

Selection of the holes grouped in any subnet for each α_{net} *(Module 2.1.3).* Performed for each of the masks $BW^{\alpha_{net}}_{holesofnet}$. Selecting holes involves the creation of a set $SetOfSubnets^{\alpha_{net}}$ according to the parameters (*numMinHoles, distMaxHoles, rangMaxSizeHole*) described in Section 2.6.2, which would contain the different subnets $Subnet^{\alpha_{net}}$.

Firstly, the different holes $C^{\alpha_{net}}_{holesofnet} \subset BW^{\alpha_{net}}_{holesofnet}$ are examined and the centroid of each one is calculated. A set $SetOfSubnets^{\alpha_{net}}$ is created, consisting of different subnets $Subnet^{\alpha_{net}}$, each of which is a group of "close" holes, i.e. whose centroids are at a shorter or the same distance as *distMaxHoles*.

Secondly, to each subnet $Subnet^{\alpha_{net}}$ of $SetOfSubnets^{\alpha_{net}}$ is applied the criterion that there is uniformity of size on a local level. In order to do so, the mean size of the subnet *meanSizeHoles* is calculated and holes $C^{\alpha_{net}}_{holesofnet}$ whose size is not between $(1 - rangMaxSizeHole).meanSizeHoles$ and $(1+rangMaxSizeHole).meanSizeHoles$ are eliminated.

Thirdly, the subnets whose number of holes is $< numMinHoles$ are eliminated from $SetOfSubnets^{\alpha_{net}}$.

As a result of this task, the $SetOfSubnets^{\alpha_{net}}$ are created, which leads to subsequent modification of the $BW^{\alpha_{net}}_{holesofnet}$ (the holes belonging to no subnet are eliminated). Each set of subnets corresponding to each value of α_{net} can be seen graphically by building a colour image of set of subnets $I^{\alpha_{net}}_{setofsubnets}$, colouring each of the subnets where the holes group, as shown in Fig. 7.

Selection of the holes belonging to the pigment network for each (α_{net}, α_{holes}) *(Module 2.1.4).* After selecting the grouped holes, this task is where the ideas put forward in the motivation Section 2.6.1 are applied. The combination of image masks obtained from probability images corresponding to the $\alpha - cuts$ obtained from the fuzzy sets is performed for each of the different combinations of values (α_{net}, α_{holes}), in the following order:

$$for(\alpha_{net} = 0.1; \alpha_{net} \leq 0.9; \alpha_{net} = \alpha_{net} + 1)\{$$
$$for(\alpha_{holes} = 0.1; \alpha_{holes} \leq 0.9; \alpha_{holes} = \alpha_{holes} + 1)\{$$
$$\ldots\}\}$$

Firstly, the holes $C^{\alpha_{net}}_{holesofnet} \subset BW^{\alpha_{net}}_{holesofnet}$ are examined and those which satisfy $\frac{|C^{\alpha_{net}}_{holesofnet} \cap BW^{\alpha_{holes}}_{holes}|}{|C^{\alpha_{net}}_{holesofnet}|} > prop$ are selected. $BW^{(\alpha_{net},\alpha_{holes})}_{selectedholes} \subset BW^{\alpha_{net}}_{holesofnet}$ is created, as the union of all the selected holes. Secondly, the selected holes $C^{\alpha_{net}}_{holesofnet} \subset BW^{(\alpha_{net},\alpha_{holes})}_{selectedholes}$ belonging to subnets $Subnet^{\alpha_{net}}$ of $SetOfSubnets^{\alpha_{net}}$ are examined so that the number of selected holes of the subnet $Subnet^{\alpha_{net}}$ is $< numMinHoles$ are eliminated. Thirdly, there are selected holes if and only if their sum is $\geq thr\_numMinTotalHoles$.

As a result of this task, the selected holes are obtained in $BW^{(\alpha_{net},\alpha_{holes})}_{selectedholes}$ in each iteration corresponding to each (α_{net}, α_{holes}). The content can be seen graphically in the image of pigment network detection $I^{(\alpha_{net},\alpha_{holes})}_{PN}[prop]$ defined in Section 2.6.1, by scaling the definition, taking into account all the parameters involved in the parameterisation, to $I^{(\alpha_{net},\alpha_{holes})}_{PN}[prop, numMinHoles, distMaxHoles, rangMaxSizeHole]$. As all the other definitions of variables made in tasks 3–6, this variable is dependent of the values of (*prop, numMinHoles, distMaxHoles, rangMaxSizeHolee*), so this notation can be relaxed to $I^{(\alpha_{net},\alpha_{holes})}_{PN}$ as shown in Fig. 7. The processing performed in this task is directly related to the following task involving feature extraction, as shall be seen.

Extraction of features (Module 2.1.5). The features that discriminate well in the pattern recognition issue are extracted in this task. To select features, a study was carried out that takes into consideration the different types of images, with and without pigment network, and how the selection of holes belonging to the pigment network works in iterations corresponding to different values of (α_{net}, α_{holes}).

It was noted that in the images that contain pigment network, both in cases in which this is very clear and in those in which it is difficult to make out, even in those in which there are few holes, it is ascertained that the existing holes of the structure are selected in many iterations, even with high probability (α_{net}, α_{holes}) values. It was also noted that in the images that do not contain pigment network nothing is selected in very clear cases and, in those in which it is less clear for different reasons –such as the presence of disturbing artefacts (e.g. hair, flashes, ruler markings or air bubbles), the presence of other dermoscopic structures (such as globules, dots, streaks, etc.) or the presence of regions of pixels with similar textures to pigment network– it is quite usual for "supposed holes" to be selected with low probability (α_{net}, α_{holes}) values but, when the probabilities increase, these "supposed holes" are no longer obtained.

This means that the model works well in discerning the pattern, even when dealing with disturbing artefacts –which means that no prior preprocessing is required in this method– and in dealing with other dermoscopic structures.

Five features are extracted taking into consideration the above observations: 1. *probNetMax*: from iterations (α_{net}, α_{holes}), the maximum α_{net} where there are selected holes; 2. *probHolesMax*: from the iterations (α_{net}, α_{holes}), with $\alpha_{net} = probNetMax$, the maximum α_{holes} where there are selected holes (evidently, this feature only makes sense when combined with *probNetMax*); 3. *numProbabilities*: number of iterations (α_{net}, α_{holes}) where there are selected holes; 4. *numHoles*: sum of all the selected holes for each of the different iterations (α_{net}, α_{holes}); 5. *numSubnets*: sum of all the groups where there are selected holes for each of the different iterations (α_{net}, α_{holes}).

Obtaining the hard classification model in order to discriminate between "absent" and "present" (Module 2.1.6). For the combination

of parameters (*prop, numMinHoles, distMaxHoles, rangMaxSizeHole*), a hard classifier is used to generate a hard classification model in order to discriminate between "absent" and "present" from the values of the features for the labelled images in the "absent" and "present" categories. The classifier used and the results obtained are explained in Section 3.2.

2.6.5. Selection of the best classification model (Module 2.2)

The different classification models corresponding to the different combinations of parameters (*prop, numMinHoles, distMaxHoles, rangMaxSizeHole*) are analysed and the best one is selected. Section 3.2 explains this in detail.

2.6.6. Diagnosis between "absent" and "present" (Module 2.3)

Having chosen the best classification model, the decision rules for the purpose of carrying out the diagnosis are obtained. The results obtained are shown in Section 3.2.

3. Results

3.1. Fuzzy detection of pixels of type "net", "hole" and "other"

As mentioned in Section 2.5.4, the purpose of the fuzzy detection of pixels is to obtain fuzzy membership rules for each of the pixels. The Weka implementation of Random Forest is used [36], which is a classifier that provides such functionality (a fuzzy classifier) and, as shall be seen, obtains very good results in terms of reliability, as well as being very fast with low computational cost. This is essential in order to make the algorithm efficient, since each of the 768×512 pixels of the different images must be computed. From a set of 9196 samples taken, 94.1%% accuracy and AUC of 0.99 were obtained using 10-fold cross-validation.

3.2. Hard classification models to discriminate between "absent" and "present" and selection of the best one. The results of the method

Different hard classification models are generated that correspond to 180 different combinations of parameters (*prop, numMinHoles, distMaxHoles, rangMaxSizeHole*) $\in \{0.5, 0.6, 0.7, 0.8, 0.9\} \times \{1, 2, 3\} \times \{10, 15, 20, 15\} \times \{0.5, 0.65, 0.8\}$. Each of them is generated by using: 1. The data set used in this work (commented in Section 2.1), consisting of 875 images, 326 "absent" and 549 "present" (this distribution of classes corresponds approximately to the percentages of both classes in the atlas [32]), from the values extracted from the 5 features {*probNetMax, probHolesMax, numProbabilities, numHoles, numSubnets*}; 2. The C4.5 decision tree classifier [37], a high-performance classifier with low computational cost, using the Weka implementation J48 [38].

In order to select the best model, the AUC (Area Under Curve) and the accuracy measures are used as criteria for validating the robustness and the reliability of the models, with the AUC proving to be particularly relevant when the data set is not balanced, as in this case [39].

Selection of the optimal subset of features so as to simplify the resulting model is also subject to analysis. As just 5 features are considered, instead of using the usual procedure (analysing each classification model and selecting its best features), it is possible to validate the different possible subsets of features separately by brute force. In order to do so, for each combination of parameters, $31 = 2^5 - 1$ classification models were generated, each one corresponding to a subset of features. Therefore, a total of $5580 = 180 * 31$ models were evaluated, using 10-fold cross-validation.

The maximum values of AUC and accuracy obtained were 0.912 and 88.91%% respectively. In seeking the best robustness and reliability, only the two models were selected that met the conditions of having a high AUC (≥ 0.9) and great accuracy ($\geq 88\%\%$):

Table 1
Results of the most relevant works in recognition of pigment network (AUC: Area Under Curve, ACC: Accuracy, SE: Sensitivity, SP: Specificity).

Methods	Images	Results
Sadeghi et al. [20]	500	94.30%% ACC
Barata et al. [23]	200	91.1%% SE, 82.1%% SP
Garcia-Arroyo et al. [24]	220	83.64%% ACC, 86%% SE, 81.67%% SP
Proposed Work	875	0.912 AUC, 88%% ACC, 90.71%% SE, 83.44%% SP

Model 1. AUC: 0.901, Accuracy: 88%%, (0.5, 20, 2, 0.65), {*numProbabilities, numHoles, numSubnets*}.

Model 2. AUC: 0.912, Accuracy: 88%%, (0.5, 20, 2, 0.8), {*numProbabilities, numHoles*}.

Obviously, the one with the highest AUC was selected, which was also the most simplified. This classification model corresponds, as shown, to both the combination of parameters (0.5, 20, 2, 0.8) and the subset of features {*numProbabilities, numHoles*}, obtaining 0.912 AUC (the maximum AUC of all models) and 88%% accuracy (very close to maximum accuracy), with 90.71%% sensitivity and 83.44%% specificity, which were selected as the method results. The feature with the greatest importance was *numProbabilities*, obtaining 0.876 AUC with the same combination of parameters (0.5, 20, 2, 0.8).

4. Discussion and conclusions

When analysing the diagnosis made in the 875 images, it can be observed that the algorithm is highly reliable and robust, succeeding even with difficult images.

Most errors correspond to images of the type discussed in requirement 6 of Section 2.2, with the presence of "borderline images" being particularly relevant. This is an inevitable source of errors in this type of study of decision systems concerning subjective patterns, as opposed, for example, to a diagnostic system which decides whether a lesion has melanoma or not, having been diagnosed histopathologically, which is purely objective in nature. Fig. 8 shows some examples of the diagnosis made by this system.

Numerical comparison between the proposed method and the most important methods in the state of the art, described in Section 1.1, are shown in Table 1. As can be seen, the proposed method contains the largest number of images in the state of the art to detect pigment network, a total of 875, and also the best results, except partly for the work by Sadeghi et al. [20], which obtains slightly greater accuracy. In order to make the most accurate comparison with this work, further data would be required regarding generation of the classification model so as to evaluate its robustness and, of course, the detailed design, the image data employed, the AUC, the sensitivity and the specificity. It should also be taken into account that –because of methodological reasons as commented in Section 2.4.2– this method performs from already segmented images, unlike the other three methods that perform from non-segmented images, although as mentioned in Section 2.4.2 the method is scarcely affected by this fact. Taking into account all these considerations –and also the innovative design of the algorithm and the other contributions– it is clear that the proposed method is an important advance in recognition of pigment network.

4.1. Conclusions

This paper describes a highly innovative method of pattern recognition for the detection of pigment network in dermoscopy images, based on fuzzy classification of pixels. This algorithm is the main contribution, and it could also be used to deal with other pattern recognition problems of a similar nature. The method was

tested on a database of 875 images –by far the largest in the state of the art in the detection of pigment network– extracted from a public Atlas of Dermoscopy, with AUC results of 0.912 and 88%% accuracy being obtained, with 90.71%% sensitivity and 83.44%% specificity, which proves its robustness and reliability. In addition, the classification model generated is simplified, consisting of two features {*numProbabilities, numHoles*}, with the feature *numProbabilities* proving to be particularly relevant. Some of the contributions made by the method in terms of the state of the art are the lack of need for prior preprocessing (e.g. of hairs) and the improvement in differentiation between the reticular structure and other dermoscopic structures, both problems that arise in most previous works on the subject. Moreover, it puts forward a new methodological approach for work of this kind –that constitutes an attempt to formalise the design of dermoscopic pattern recognition methods in a more optimal way– introducing the system specification as a required step prior to algorithm design, being this specification the basis for a required parameterisation –in the form of configurable parameters (with their value ranges) and set threshold values– of the algorithm and the subsequent conducting of the experiments. This algorithm can be integrated into a CAD for the automated detection of melanoma –for example, using the "ABCD Rule"– and used in different environments: medical centers (eg primary medicine), telemedicine web platforms, smartphone apps, etc.

Conflict of interest

None Declared

Acknowledgments

This work has been carried out with the collaboration of J.L. Diaz and J.Gardeazabal, dermatologists from Cruces Hospital in Bilbao (Basque Country, Spain). This research was partially funded by the Basque Government Department of Education (eVIDA Certified Group IT579-13).

References

[1] J. Malvehy, S. Puig, G. Argenziano, A.A. Marghoob, H.P. Soyer, Dermoscopy report: proposal for standardization. results of a consensus meeting of the international dermoscopy society., J. Am. Acad. Dermatol. 57 (1) (2007) 84–95, doi:10.1016/j.jaad.2006.02.051.
[2] L. Andreassi, R. Perotti, P. Rubegni, M. Burroni, G. Cevenini, M. Biagioli, P. Taddeucci, G. Dell'Eva, P. Barbini, Digital dermoscopy analysis for the differentiation of atypical nevi and early melanoma: a new quantitative semiology, Arch. Dermatol. 135 (12) (1999) 1459–1465.
[3] P. Rubegni, G. Cevenini, M. Burroni, R. Perotti, G. Dell'Eva, P. Sbano, C. Miracco, P. Luzi, P. Tosi, P. Barbini, et al., Automated diagnosis of pigmented skin lesions, Int. J. Cancer 101 (6) (2002) 576–580.
[4] A. Masood, A. Ali Al-Jumaily, Computer aided diagnostic support system for skin cancer: a review of techniques and algorithms, Int. J. Biomed. Imaging 2013 (2013).
[5] G. Argenziano, H. Soyer, S. Chimenti, E. Al., Dermoscopy of pigmented skin lesions: results of a consensus meeting via the internet, J. Am. Acad. Dermatol. 48 (5) (2003). 693–679
[6] H. Ganster, A. Pinz, R. Röhrer, E. Wildling, M. Binder, H. Kittler, Automated melanoma recognition., IEEE Trans Med Imaging 20 (3) (2001) 233–239.
[7] C. Serrano, B. Acha, Pattern analysis of dermoscopic images based on markov random fields, Pattern Recognit. 42 (6) (2009) 1052–1057.
[8] Q. Abbas, M.E. Celebi, C. Serrano, I. Fondón, G. Ma, Pattern classification of dermoscopy images: a perceptually uniform model, Pattern Recognit. 46 (1) (2013) 86–97.
[9] M. Sadeghi, T. Lee, H. Lui, D. McLean, S. Atkins, Detection and analysis of irregular streaks in dermoscopic images of skin lesions, IEEE Trans. Med. Imaging 32 (5) (2013) 849–861.
[10] H.P. Soyer, G. Argenziano, R. Hofmann-Wellenhof, Color Atlas of Melanocytic Lesions of the Skin, Springer, 2007.
[11] J.L. García Arroyo, B. García Zapirain, Comparison of image processing techniques for reticular pattern recognition in melanoma detection, in: M.E. Celebi, T. Mendonça, J.S. Marques (Eds.), Dermoscopy Image Analysis, CRC Press/Taylor & Francis, 2015, pp. 131–181, doi:10.1201/b19107-6.
[12] S. Fischer, P. Schmid, J. Guillod, Analysis of skin lesions with pigmented networks, in: 1996 International Conference on Image Processing, 1, IEEE, Lausanne, Switzerland, 1996, pp. 323–326.
[13] M.G. Fleming, C. Steger, A.B. Cognetta, J. Zhang, Analysis of the network pattern in dermatoscopic images, Skin Res. Technol. 5 (1) (1999) 42–48.
[14] C. Grana, V. Daniele, G. Pellacani, S. Seidenari, R. Cucchiara, Network patterns recognition for automatic dermatologic images classification, in: Medical Imaging, 2007 International Society for Optics and Photonics, San Diego, California, United States, 2007, p. 65124C.
[15] A. Gola Isasi, B. García Zapirain, A. Mendez Zorrilla, Melanomas non-invasive diagnosis application based on the ABCD rule and pattern recognition image processing algorithms, Comput. Biol. Med. 41 (9) (2011) 742–755.
[16] Q. Abbas, M.E. Celebi, I. Fondón, W. Ahmad, Melanoma recognition framework based on expert definition of ABCD for dermoscopic images, Skin Res. Technol. 19 (1) (2013) e93–e102.
[17] B. Caputo, V. Panichelli, G.E. Gigante, Toward a quantitative analysis of skin lesion images, Stud. Health Technol. Inform. 90 (2002) 509–513.
[18] T. Tanaka, S. Torii, I. Kabuta, K. Shimizu, M. Tanaka, Pattern classification of nevus with texture analysis, IEEJ Trans. Electr. Electron. Eng. 3 (1) (2008) 143–150.
[19] G. Di Leo, C. Liguori, A. Paolillo, P. Sommella, An improved procedure for the automatic detection of dermoscopic structures in digital ELM images of skin lesions, in: 2008 IEEE Conference on Virtual Environments, Human–Computer Interfaces and Measurement Systems, IEEE, Istanbul, Turkey, 2008, pp. 190–194.
[20] M. Sadeghi, M. Razmara, T.K. Lee, M.S. Atkins, A novel method for detection of pigment network in dermoscopic images using graphs, Comput. Med. Imaging Graph. 35 (2) (2011) 137–143.
[21] M. Sadeghi, M. Razmara, P. Wighton, T.K. Lee, M.S. Atkins, Modeling the dermoscopic structure pigment network using a clinically inspired feature set, Lect. Notes Comput. Sci. 6326 (2010) 467–474.
[22] P. Wighton, T.K. Lee, H. Lui, D.I. McLean, M.S. Atkins, Generalizing common tasks in automated skin lesion diagnosis., IEEE Trans. Inf. Technol. Biomed. 15 (4) (2011) 622–629.
[23] C. Barata, J.S. Marques, J. Rozeira, A system for the detection of pigment network in dermoscopy images using directional filters, IEEE Trans. Biomed. Eng. 59 (10) (2012) 2744–2754.
[24] J.L. García Arroyo, B. García Zapirain, Detection of pigment network in dermoscopy images using supervised machine learning and structural analysis, Comput. Biol. Med. 44 (2014) 144–157, doi:10.1016/j.compbiomed.2013.11.002.
[25] W. Barhoumi, A. Baâzaoui, Pigment network detection in dermatoscopic images for melanoma diagnosis, IRBM 35 (3) (2014) 128–138.
[26] B. Shrestha, J. Bishop, K. Kam, X. Chen, R.H. Moss, W.V. Stoecker, S. Umbaugh, R.J. Stanley, M.E. Celebi, A.A. Marghoob, G. Argenziano, H.P. Soyer, Detection of atypical texture features in early malignant melanoma, Skin Res. Technol. 16 (1) (2010) 60–65.
[27] M. Machado, J. Pereira, R. Fonseca-Pinto, Classification of reticular pattern and streaks in dermoscopic images based on texture analysis, J. Med. Imaging 2 (4) (2015) 044503.
[28] Q. Abbas, M.E. Celebi, I. Fondón, Computer-aided pattern classification system for dermoscopy images, Skin Res. Technol. 18 (3) (2012) 278–289.
[29] M. Anantha, R.H. Moss, W.V. Stoecker, Detection of pigment network in dermatoscopy images using texture analysis, Comput. Med. Imaging Graph. 28 (5) (2004) 225–234.
[30] A. Saez, C. Serrano, B. Acha, Model-based classification methods of global patterns in dermoscopic images, IEEE Trans. Med. Imaging 33 (5) (2014) 1137–1147.
[31] M. Machado, J. Pereira, R. Fonseca-Pinto, Reticular pattern detection in dermoscopy: an approach using curvelet transform, Res. Biomed. Eng. 32 (2) (2016) 129–136.
[32] G. Argenziano, H.P. Soyer, V.D.G.D. Piccolo, P. Carli, M. Delfino, A. Ferrari, R. Hofmann-Wellenhof, D. Massi, G. Mazzocchetti, M. Scalvenzi, I.H. Wolf, Interactive atlas of dermoscopy, EDRA-Medical Publishing and New Media, Milan, Italy, 2000.
[33] J.L. Garcia-Arroyo, B. Garcia-Zapirain, Segmentation of skin lesions based on fuzzy classification of pixels and histogram thresholding, arXiv preprint arXiv:1703.03888 (2017).
[34] R.C. Gonzalez, R.E. Woods, Digital Image Processing, 3rd edition, Prentice Hall, 2008.
[35] M. Petrou, P. García Sevilla, Image Processing: Dealing With Texture, John Wiley & Sons, 2006.
[36] L. Breiman, Random forests, Mach. Learn. 45 (1) (2001) 5–32.
[37] J.R. Quinlan, C4.5: Programs for Machine Learning, 1, Morgan Kaufmann, San Francisco, CA, 1993.
[38] The University of Waikato, WEKA: Data Mining Software in Java, 2016, (http://www.cs.waikato.ac.nz/ml/weka). Accessed: 2016-12-20.
[39] J. Huang, C.X. Ling, Using AUC and accuracy in evaluating learning algorithms, IEEE Trans. Knowl. Data Eng. 17 (3) (2005) 299–310.